

A cascading influence of calcium carbonate on the biogeochemistry and pedogenic trajectories of subalpine soils, Switzerland

Mike C. Rowley^{a,*}, Stephanie Grand^a, Thierry Adate^b, Eric P. Verrecchia^a

^a IDYST – Institute of Earth Surface Dynamics, Faculty of Geosciences and Environment, Université de Lausanne, Switzerland

^b ISTE – Institute of Earth Sciences, Faculty of Geosciences and Environment, Université de Lausanne, Switzerland

ARTICLE INFO

Handling Editor: David Laird

Keywords:

Pedogenic inertia
Pedogenic thresholds
Soil inorganic carbon
Soil organic carbon
Pedogenic oxides

ABSTRACT

Soil research in temperate to cool and humid regions has typically focused on acidic soils; there has been relatively little investigation of the effects of calcium carbonate (CaCO₃) on unamended soil properties or function in these environments. The object of this study was to characterise the effects of small amounts of CaCO₃ on pedogenic trajectories and soil biogeochemistry in a humid subalpine valley of Switzerland. To isolate the influence of CaCO₃, six profiles were selected that had developed under almost identical conditions for soil formation, *i.e.* climate, topography, vegetation structure, time since deglaciation, silicate mineralogy and texture. The main difference between the profiles was that three contained a small quantity of CaCO₃ (< 6.2%; thereafter, ‘CaCO₃-bearing’) while the remaining three contained no detectable CaCO₃ (thereafter, ‘CaCO₃-free’). The presence of CaCO₃ was associated with cascading changes in soil biogeochemistry. These changes included higher pH, an order of magnitude higher extractable Ca and twice as much soil organic carbon (SOC). CaCO₃-bearing profiles also displayed a higher proportion of poorly crystalline Fe forms. The higher pH at the CaCO₃-bearing site was attributable to the weak buffering provided by CaCO₃ dissolution, which in turn maintained the relatively higher extractable Ca. Exchangeable Ca (Ca_{Exch}) and other reactive Ca forms could help stabilise SOC, contributing to its accumulation through processes such as flocculation and subsequent occlusion within aggregates and/or sorption to mineral surfaces. The increased SOC, Ca_{Exch} and pH at the CaCO₃-bearing site could in turn be inhibiting the crystallisation of disordered Fe forms, but further research is required to confirm this effect and isolate the exact mechanisms. Overall, this study shows that the presence of small amounts of CaCO₃ in humid environments has a far-reaching influence on soil biogeochemistry and further supports the idea that indicators of Ca prevalence have the potential to improve regional SOC estimates.

1. Introduction

Calcium carbonate (CaCO₃) accounts for an important fraction of C present in soils, linking the long-term geological C cycle with the faster biogeochemical cycling of soil organic carbon (SOC; Gao et al., 2017; Hasinger et al., 2015; Sanderman, 2012; Zamanian et al., 2016). Globally, the presence of CaCO₃ in soils is inversely correlated to effective precipitation because of its susceptibility to chemical weathering (Arkley, 1963; Jenny, 1941; Slessarev et al., 2016). However, there remains clear outliers in this global correlation, as CaCO₃-bearing soils can be found in humid environments and are typically related to lithological CaCO₃ reservoirs that are yet to be exhausted by leaching (Slessarev et al., 2016). Furthermore, while the precipitation of CaCO₃ by physicochemical processes is not typically favoured in humid or acidic environments (Barta et al., 2018; Cerling, 1984), it can still occur

through the direct and indirect results of biological processes (Bindschedler et al., 2016; Cailleau et al., 2005; Hasinger et al., 2015). Thus, CaCO₃ in soils can persist in a state of disequilibrium with climate, when driven by reserves of calcareous parent material or biological processes.

The aforementioned disequilibrium is an example of pedogenic inertia, defined as the persistence of certain soil conditions or processes in spite of the presence of extrinsic pedogenic factors that favour their discontinuation (Bryan and Teakle, 1949). The extrinsic pedogenic factors refer to four of the five conventional factors of pedogenesis (parent material, biota, topography and climate; Jenny, 1941), excluding time which acts as a vector (Muhs, 1984). In the previously used example, the state of pedogenic inertia exists because an intrinsic pedogenic factor, the continued and slow dissolution of CaCO₃, prevents the expression of an acidic soil favoured since deglaciation by the

* Corresponding author at: Bureau 4633, Bâtiment Geopolis, UNIL Quartier Mouline, Lausanne 1015, Switzerland.

E-mail address: mike.rowley@unil.ch (M.C. Rowley).

<https://doi.org/10.1016/j.geoderma.2019.114065>

Received 21 August 2019; Received in revised form 29 October 2019; Accepted 30 October 2019

Available online 03 December 2019

0016-7061/ © 2019 The Authors. Published by Elsevier B.V. This is an open access article under the CC BY-NC-ND license

(<http://creativecommons.org/licenses/by-nc-nd/4.0/>).

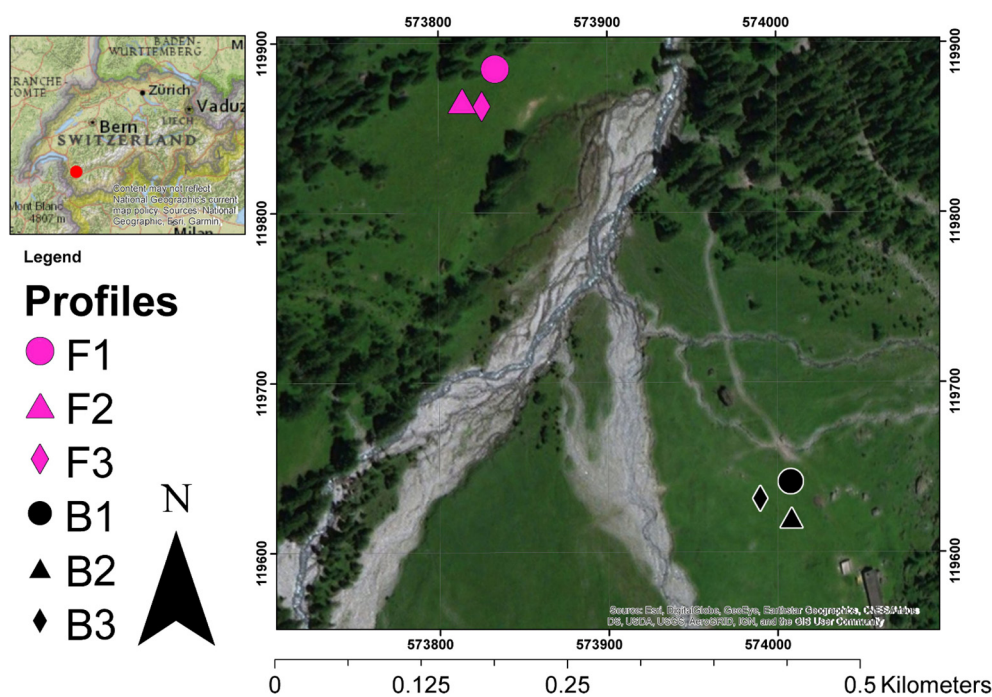


Fig. 1. Profile locations in the Nant valley, Vaud Alps, Switzerland. Coordinates are in CH1903 LV03 (ESRI, 2019). Profiles labelled with an F (F1, F2, F3) are at the CaCO_3 -free site and profiles labelled with a B (B1, B2, B3) are at the CaCO_3 -bearing site.

extrinsic factor of climate (Chadwick and Chorover, 2001). In turn, this inertia can diverge the trajectory of pedogenesis, as evidenced by the wide array of soils that develop on parent material containing varied CaCO_3 content in humid or mountainous environments (Kowalska et al., 2019). Unless there is a change in extrinsic factors, pedogenic inertia is by nature a transient condition that will eventually cease in a threshold response. Pedogenic thresholds are defined as limits in intrinsic pedogenic factors or soil properties, that once breached, cause rapid and irreversible transformations in pedogenesis and biogeochemistry (Chadwick and Chorover, 2001; Muhs, 1984). In the case of CaCO_3 , a threshold may occur when its concentration becomes too low to provide pH buffering to the soil system, triggering changes in soil biogeochemistry.

The presence of CaCO_3 plays a commanding role in governing soil biogeochemistry. The primary mechanism for this is the buffering of soil pH caused by the consumption of H^+ during acid hydrolysis of CaCO_3 (Bache, 1984; Zamanian et al., 2016). pH is known as a master variable in soil ecosystems and impacts many biological and chemical processes, such as the composition of microbial communities (Bahram et al., 2018; Rousk et al., 2010), mineral weathering rates (Chadwick and Chorover, 2001), redox chemistry (Bartlett and James, 1993) and the speciation and lability of many elements (Sposito, 2016). The dissolution of CaCO_3 also provides a continued supply of Ca^{2+} , which has long been thought to promote the accumulation of SOC in CaCO_3 -bearing soils through occlusion (Grant et al., 1992; Muneer and Oades, 1989) and sorption processes (Edwards and Bremner, 1967; Kalinichev and Kirkpatrick, 2007; see review in Rowley et al., 2018). Recent evidence has highlighted a potential stabilisation of SOC by Fe-Ca-ternary complexation (Sowers et al., 2018a,b), which could be more prevalent in CaCO_3 -bearing soils than acidic profiles with limited exchangeable Ca (Ca_{Exch}). However, further research is still needed to evidence links between Ca, SOC, and reactive forms of Fe in different soil environments. In particular, the effects of small amounts of CaCO_3 , commonly found in cool humid edaphic environments, on soil biogeochemistry still require further investigation.

Therefore, the objective of this paper is to quantify the impact of small amounts of CaCO_3 on the pedogenesis and biogeochemistry of

soils in a humid environment (Nant Valley, Vaud Alps, Switzerland). To isolate the effects of CaCO_3 on pedogenesis at the Nant Valley, six soil profiles were selected that had developed under near-identical conditions for soil formation (Jenny, 1941) or extrinsic pedogenic factors (Chadwick and Chorover, 2001; Muhs, 1984), except that three profiles contained a small quantity of CaCO_3 ($< 6.2\%$ CaCO_3) while the other three were devoid of carbonates. Our hypothesis was that the presence or absence of CaCO_3 would trigger a threshold response, resulting in large divergences in pedogenesis and soil biogeochemistry, particularly regarding the accumulation of SOC.

2. Materials and methods

2.1. Site description and sampling

This study was completed in the Nant Valley (573'000, 119'000 CH1903 LV03), a partially glaciated watershed in the Vaud Alps, Switzerland. The valley is orientated north-south and situated on the Morcles Nappe, a near-recumbent anticline consisting of Jurassic and Cretaceous shallow-water limestones intercalated with marl and shale deposits (Austin et al., 2008). Sampling took place in a pastoral area of the valley floor (ca. 1500 m elevation above sea level), which is lightly-grazed by heifers during summer months. This area receives approximately 1800 mm yr^{-1} precipitation, has a mean annual temperature of $6 \text{ }^\circ\text{C}$ (Vittoz and Gmür, 2008) and is typically covered in snow from December to April.

Two sampling sites were selected that represented a range of CaCO_3 contents, while having developed under near-identical soil forming conditions. Potential variations in the CaCO_3 content were identified in the field using an auger, 10% v/v HCl and a field pH meter (Hellige pH Indicator). Retained sites were located on subalpine prairies and thus had the same vegetation structure, which had previously been characterised in detail (Grand et al., 2016; Vittoz and Gmür, 2008). Soils at each site developed in mixed alluvial, morainic and colluvial materials issued from the Morcles Nappe (Grand et al., 2016; Perret and Martin, 2014), deposited around the time of the retreat of the Martinets Glacier (ca. 15 Ka; Seguinot et al., 2018). Sites all had a minimal slope, the

same altitude, similar climate due to their proximity to each other (ca. 400 m apart) and equivalent irradiance.

Three profiles were dug at each sampling site in July–August 2016 (Fig. 1). Profiles were classified as Eutric Cambisols (siltic) with no HCl effervescence on the northwest bank and Cambic Phaeozems (siltic) that effervesced on the southeast bank of the Nant River (IUSS Working Group WRB, 2015). For brevity, the Eutric Cambisols will henceforth be labelled as CaCO₃-free (profiles F1, F2, F3, in fuchsia) and the Cambic Phaeozems will be labelled as CaCO₃-bearing (profiles B1, B2, B3, in black). Profiles were sampled at 6–7 depth intervals (Table 1) to a maximum depth of 50 cm, sampling the deepest layers first to prevent intra-profile contamination. Samples were labelled from 1 to 6 / 7 with increasing depth (e.g., F1.1-to-F1.6) and then transported to the University of Lausanne in sealed bags. Aboveground biomass (AGB) was also randomly sampled from the sites to quantify potential differences in vegetative inputs at the sites.

2.2. Laboratory analyses

Samples were air-dried and sieved to 2 mm. All analyses were completed on this fine earth fraction unless stated otherwise and results were corrected for residual humidity (van Reeuwijk, 2002). Sub-samples were ground to a fine powder (ca. 20 µm) for 3 min in an agate crucible with a vibrating-disc mill (Siebtechnik Schibenschwingmuhle-TS). AGB samples were oven-dried (40 °C), ground by hand and homogenised for further analysis. Quality control procedures included the analysis of an internal standard when appropriate, as well as the inclusion of blanks and quality checks. A minimum of 10% blind replicates were included in all analyses. All plastic and glassware were acid washed (3 M HCl) to remove trace contamination.

2.2.1. pH and texture

Soil pH was measured potentiometrically using a glass-body combination electrode (Thermo Scientific Orion ROSS Probe) on field moist samples in a 0.1 M CaCl₂ solution (1:2 soil:solution mass ratio). Texture was determined using laser diffraction (0.01–2000 µm; Pansu and Gautheyrou, 2006). Pre-treatment included digestion of soil organic matter with increasing concentrations of H₂O₂ (10–35%). During the procedure, pH was kept around neutrality with NaOH to prevent destruction of mineral components due to acidification. Samples were then shaken with sodium hexametaphosphate for 16 h to chemically disperse particles prior to measurement with a Beckman Coulter LS13320 Particle Sizing Analyser. The analyser pump speed was set at 80% (ca. 9500 mL min⁻¹) and samples were weakly sonicated in both the auto-sampler and analyser (4/8 setting; ca. 2 J mL⁻¹) prior to measurement. The analyser was run using the default optical model (Fraunhofer.rf780d) in auto-dilution mode. Measurements were taken when an obscuration of 12% was attained.

2.2.2. Elemental analysis

The total elemental composition was quantified on ground samples using X-ray fluorescence (XRF; PANalytical PW2400 WDXRF Spectrometer) following lithium tetraborate fusion (PANalytical Perl X3 Fuser). Results were corrected for loss-on-ignition at 1050 °C (Solo 111–13/10/30). Organic C and total nitrogen were quantified on AGB and soil ground samples by dry combustion (Carlo Erba 1108 and Thermo Scientific Flash 2000 CHN Elemental Analysers). Soil samples were fumigated for 24 h with 12 M HCl in order to remove inorganic C prior to CHN elemental analysis (Harris et al., 2001; Ramnarine et al., 2011). Samples were weighed to the nearest milligram before and after fumigation to correct for mass changes. All samples gained mass due to the formation of small quantities of chloride green rust, likely formed from the reaction of Fe oxides with Cl⁻ (Ramnarine et al., 2011).

2.2.3. Mineralogy

Bulk mineralogy was determined on ground samples prepared

according to Adatte et al. (1996) using X-ray diffraction (XRD; Thermo ARL X'TRA Powder Diffractometer). Approximately 800 mg of ground sample was pressed (20 bars) in a powder holder covered with blotting paper. Pressed samples were then analysed using Cu Kα radiation at 45 kV / 40 mA with a 13 s counting time per 0.02° for 2 θ in the 1–65° range. Samples were rotated at a range of 1° min⁻¹ with an acquisition step size of 0.03 – 0.05° 2 θ using a 0 / 0 type goniometer with a 250 mm radius. A spectral counter (Thermo ARL Water-cooled Silicon Detector) was used to eliminate Cu Kβ and Fe parasitic emissions. The bulk mineralogy of samples was then quantified using external standards (Adatte et al., 1996).

Samples from a randomly selected profile at each site were also prepared for clay mineralogical analysis according to Adatte et al. (1996). Briefly, samples from profiles F1 and B2 were mixed with deionised water, agitated, and combined with 10% HCl to remove carbonates. Insoluble residues were washed by centrifugation until neutral pH was acquired. Different size fractions (< 2 µm and < 16 µm) were separated by sedimentation according to Stokes' law. Selected fractions were then pipetted onto glass plates and air-dried. Resulting oriented slides were analysed by XRD before and after ethylene glycol solvation (heating to 450 °C).

Total carbonate content expressed as CaCO₃ equivalent material (CCE) was determined using a weak acid dissolution followed by measurement of the pH of the extractant (Loeppert et al., 1984). The method was selected for its reproducibility in quantifying low amounts of CaCO₃, for which the XRD detection limit is around 1% (Loeppert and Suarez, 1996). The method was also adapted to measure reactive carbonates, by measuring extracts shortly after the addition of the weak acid. Briefly, 2 g of soils were placed in 50 mL centrifuge tubes and shaken on a rotary shaker (250 rpm) with 25 mL 0.4 M acetic acid. Holes approximately 1 mm in diameter were made in the lids to allow for degassing during the reaction. The pH of standards (reagent grade CaCO₃) and samples solutions was measured (Thermo-Fisher Scientific Orion Star A111 Probe) at 1 h (reactive carbonates) and 16 h (total carbonate) after the addition of acetic acid. Quality control was assured by running blind, analytical and spiked replicates (Loeppert and Suarez, 1996).

2.2.4. Extractable cations

Fe and Al present in pedogenic oxides were extracted using a citrate-bicarbonate dithionite solution (Fe_d or Al_d; Mehra and Jackson, 1958), while poorly crystalline and monomeric Fe and Al forms were extracted with an oxalate solution (Fe_o or Al_o; McKeague and Day, 1966). The ratio of oxalate-to-dithionite extractable Fe (Fe_o/Fe_d) was used as a measure of the crystallinity of Fe oxides (Skjemstad et al., 1992). One surficial sample (B3.1) contained more Fe_o than Fe_d (ca. 20%; Table 1). The citrate-bicarbonate dithionite extraction is typically less selective and extracts more Fe than the oxalate extraction (Dahlgren, 1994), but it can be less efficient at extracting chelated Fe (Rennert, 2019), potentially explaining the Fe_o/Fe_d ratio > 1.

Exchangeable cations were extracted from field moist samples using a 0.0166 M cobalt hexamine (Cohex; [Co(NH₃)₆]Cl₃) extraction (Aran et al., 2008). Pre-testing demonstrated that this extraction was the least aggressive towards carbonates (data not shown). Cation exchange capacity (CEC_{SUM}) was calculated as the sum of extracted exchangeable cations (cmol_c kg⁻¹), excluding H⁺. Ca was also quantified in several other soil extracts including, in order of expected increasing extraction strength: deionised water (1:4 ratio; Tirmizi et al., 2006), 2 M KCl (1:5 ratio; Keeney and Nelson, 1982), 0.05 M disodium EDTA (1:20 ratio; Lo and Yang, 1999) and 0.5 M CuCl₂ extraction (1:10 ratio; Barra et al., 2001). All extracts were vacuum-filtered (0.45 µm) and diluted with 2% HNO₃ prior to analysis on an ICP-OES (Perkin Elmer Optima 8300 Inductively Coupled Plasma–optical Emission Spectrometer).

2.3. Statistical analyses of soil variables

The effects of CaCO_3 on soil variables were investigated using linear mixed models in SAS 9.4™. The estimation method was set to restricted (residual) maximum likelihood. Conditional residuals were plotted against predicted values to evaluate deviations from homoscedasticity and goodness of fit. Residuals were also checked for normality with QQ-plots (Galecki and Burzykowski, 2015). The significance of fixed effects was evaluated using type III F-tests. The denominators' degrees of freedom were computed using the Satterthwaite adjustment (Satterthwaite, 1946). For significant fixed effects, comparison of means was carried out using t-tests without multiple inference adjustment (Webster, 2007). The alpha level of significance was set at $\alpha = 0.05$ for all tests. All reported means are conditional least-square means \pm the standard error of the mean (SEM). Means for profiles are the unweighted average of sampling intervals.

Models included site (CaCO_3 -bearing or free), depth classes and their interaction as fixed effects. Observations were blocked by profile and a different variance was computed for each site since observations from the CaCO_3 -bearing site typically had a higher dispersion than those from the CaCO_3 -free site. For extractable Fe, dispersion was also higher for surface samples and the variance was additionally allowed to vary with depth. To account for the autocorrelation of observations within profiles, depth was set as a repeated measure effect with a first-order autoregressive covariance structure. Choice of covariance structure was made based on the Bayesian Information Criteria.

A Pearson's correlation coefficient heat map was created to explore linear associations between variables using the Corrplot Package (Wei and Simko, 2017) in R (2019). Variables in the heat map were ordered hierarchically into two separate groups using the complete-linkage method (Sørensen, 1948). A principal component analysis (PCA) was conducted on the correlation matrix to synthesise relationships between variables. A factor analysis was completed on the first 5 principal components (accounting for > 82% of variance) using a quartimax orthogonal rotation (Neuhauser and Wrigley, 1954). The purpose of the quartimax rotation is to minimise the number of original variables associated with each factor to simplify interpretation. Observations were then plotted according to their factor 1 and 2 scores in Matlab®.

Finally, differences in the shape of the depth curve of SOC between the sites were explored by examining scatterplots of SOC versus depth. Linear regressions were fitted to the data for each site. A higher root mean square error (RMSE) was considered as an indication of lack-of-fit (departure from the linear trend). Residuals from the linear regression were also tested for normality using the Shapiro-Wilk test, with departures from normality used as another indicator of deviation from the linear trend.

3. Results

3.1. Soil texture, composition and silicate mineralogy

Soil texture was similar between the two sites (Fig. 2). All samples had a silty-loam texture and were comprised of six predominant textural populations (Suppl. Fig. 1). There was slightly less silt at the CaCO_3 -free site than at the CaCO_3 -bearing site ($67.3 \pm 0.7\%$ versus $74.1 \pm 0.4\%$), and consequently more sand- ($15 \pm 0.8\%$ versus $10.6 \pm 0.5\%$) and clay-sized particles ($17.8 \pm 0.3\%$ versus $15.3 \pm 0.3\%$). The surficial samples of F1 and F2 (F1.1, F2.1, F2.2 and F2.3) as well as one deep sample (F2.6) had a more pronounced peak in the fine sand population (Suppl. Fig. 1), which occurred at the expense of fine silt populations.

Major elemental compositions were mostly similar at both sites (Suppl. Table 1). Ti and other transition/post-transition metals were largely invariant. The main differences pertained to Ca, which was approximately an order of magnitude higher at the CaCO_3 -bearing site ($14.7 \pm 3.3 \text{ g kg}^{-1}$) than at the CaCO_3 -free site ($1.9 \pm 0.2 \text{ g kg}^{-1}$).

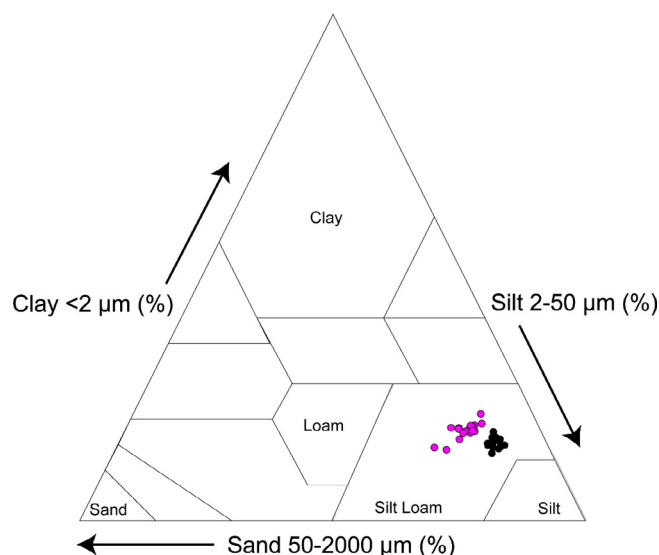


Fig. 2. Texture of samples from the CaCO_3 -free (fuchsia dots) and CaCO_3 -bearing (black dots) profiles.

There was a corresponding decrease in Si at the CaCO_3 -bearing site ($299.8 \pm 1.5 \text{ g kg}^{-1}$), relative to the CaCO_3 -free site ($318.3 \pm 3.4 \text{ g kg}^{-1}$). There were also small differences in the amounts of other elements including Mg and P, which were slightly higher at the CaCO_3 -bearing site ($14.9 \pm 0.1 \text{ g kg}^{-1}$ Mg; $4.9 \pm 0.8 \text{ g kg}^{-1}$ P) than at the CaCO_3 -free site ($12.7 \pm 0.3 \text{ g kg}^{-1}$ Mg; $1.4 \pm 0.1 \text{ g kg}^{-1}$ P). K was also marginally higher at the CaCO_3 -bearing site ($26.9 \pm 0.3 \text{ g kg}^{-1}$ versus $23.4 \pm 0.9 \text{ g kg}^{-1}$), while Na was slightly higher at the CaCO_3 -free site ($7.8 \pm 0.0 \text{ g kg}^{-1}$ versus $6.4 \pm 0.1 \text{ g kg}^{-1}$). Overall, the main difference in major elements composition between the sites consisted of an increase in Ca at the expense of Si in the CaCO_3 -bearing profiles.

Silicate mineralogy was also similar between the CaCO_3 -bearing and CaCO_3 -free sites (Suppl. Table 2). Both sites had a bulk mineralogy that was predominated by quartz (38–41%) and phyllosilicates (42–44%), with small amounts of Na-plagioclase (5%), K-feldspar (2%) and goethite (1%), while 8% of the diffraction signal remained unquantified. Average Na-plagioclase content was slightly higher at the CaCO_3 -free site ($6.1 \pm 0.2\%$) relative to the CaCO_3 -bearing ($4.8 \pm 0.3\%$), while average content of K-feldspar was marginally higher at the CaCO_3 -bearing site ($2.2 \pm 0.1\%$) relative to the CaCO_3 -free site ($1.5 \pm 0.2\%$). The phyllosilicate mineralogy was also remarkably similar between the two sites and consistent throughout the analysed profiles. The phyllosilicate population in both the randomly selected profiles (F1 and B2) was predominantly formed of chlorite and mica, with a small quantity of illite-vermiculite mixed layer minerals.

3.2. Soil pH, CaCO_3 and Ca forms

Soil pH was higher at the CaCO_3 -bearing site (range = 5–6.5) than the CaCO_3 -free (range = 4–4.6). pH also increased significantly with depth at both sites (Table 1). The amount of CaCO_3 equivalent material (CCE) was below detectable limits in profiles from the CaCO_3 -free site. Profiles from the CaCO_3 -bearing site typically contained about 0.5% reactive CCE and 0.8% total CCE (Fig. 3), except for four samples, also identified by XRD, which contained several percent of CaCO_3 . These four samples consisted of two surficial samples (B1.1, B1.2) and two of the deepest samples (B2.6, B3.7). The overall proportion of reactive carbonates, operationally-defined as having reacted with 0.4 M acetic acid in under 1 h, was high ($74.4 \pm 3.7\%$ average; Suppl. Table 2).

As with total Ca, extractable Ca was approximately an order of magnitude higher at the CaCO_3 -bearing than at the CaCO_3 -free site

Table 1

Selected properties of the study profiles at the Nant valley. Profiles F1, F2 and F3 are Eutric Cambisols (CaCO₃-free) and profiles B1, B2 and B3 are Cambic Phaeozems (CaCO₃-bearing).

Sample name	Depth intervals (cm)	Genetic Horizons	pH	Al _{Exch}	Ca _{Exch}	CEC _{sum}	Ca _{Exch} saturation	Al _{Exch} saturation	TON	SOC	C:N ratio	Al _o	Fe _o	Al _d	Fe _d	Fe _o /Fe _d ratio
				cmol _c kg ⁻¹	cmol _c kg ⁻¹	cmol _c kg ⁻¹	%	%				g kg ⁻¹	g kg ⁻¹	g kg ⁻¹	g kg ⁻¹	
F1.1	0–5	Ah	4.1	0.4	6.2	7.3	84.9	5.7	0.6	4.7	8.0	2.6	13.2	3.2	24.0	0.6
F1.2	5–10	A1	4.3	0.3	4.5	5.3	84.9	6.4	0.4	3.0	7.5	2.8	12.5	3.3	23.0	0.5
F1.3	10–15	A2	4.3	0.2	4.1	4.7	87.0	5.2	0.3	2.3	7.3	3.1	11.8	3.3	22.3	0.5
F1.4	15–25	B1	4.5	0.2	3.8	4.6	82.8	5.1	0.2	1.6	6.8	2.6	12.1	3.8	24.6	0.5
F1.5	25–35	B2	4.5	0.2	4.1	4.6	89.1	4.5	0.2	1.3	6.1	2.9	11.2	3.9	25.4	0.4
F1.6	35–52	B3	4.6	0.1	4.3	4.6	93.3	1.5	0.2	0.9	5.3	2.5	9.1	3.0	22.8	0.4
F2.1	0–5	Ah	4.0	1.3	4.4	6.1	72.6	20.6	0.7	5.8	8.6	2.9	11.1	3.7	23.7	0.5
F2.2	5–10	A	4.2	1.5	1.6	3.2	48.4	45.7	0.3	2.4	7.7	3.1	11.5	3.6	22.1	0.5
F2.3	10–15	AB	4.2	1.4	1.5	3.0	50.0	44.5	0.3	2.3	7.5	2.8	10.6	3.9	23.1	0.5
F2.4	15–20	B1	4.3	1.0	1.7	2.8	61.1	36.7	0.3	2.0	7.3	2.9	10.8	3.7	21.8	0.5
F2.5	20–25	B2	4.4	0.9	1.6	2.6	62.9	34.5	0.2	1.5	6.7	2.8	9.9	3.9	23.3	0.4
F2.6	25–40	BC	4.4	0.8	1.6	2.5	63.5	33.1	0.2	1.0	5.6	2.1	7.4	3.0	19.7	0.4
F3.1	0–5	Ah	4.3	0.5	7.6	9.0	84.1	5.7	0.7	6.1	8.5	2.8	12.2	3.3	21.7	0.6
F3.2	5–10	A	4.4	0.9	3.2	4.5	71.2	19.8	0.4	3.4	7.8	3.0	11.6	3.6	21.8	0.5
F3.3	10–15	B1	4.5	0.9	2.6	3.8	66.9	23.5	0.3	2.3	7.4	2.7	9.9	3.6	21.5	0.5
F3.4	15–20	B2	4.4	1.1	1.7	3.0	56.4	34.8	0.3	2.0	7.3	3.0	10.6	4.3	24.6	0.4
F3.5	20–25	B3	4.5	1.1	1.9	3.2	58.1	33.8	0.2	1.7	7.4	3.2	10.5	4.1	22.9	0.5
F3.6	25–40	BC	4.5	1.1	1.7	3.1	54.3	35.9	0.2	1.5	7.5	3.2	10.1	3.8	20.5	0.5
B1.1	0–5	Ah1	6.3	0	23.2	23.7	97.6	0.0	0.8	7.7	9.2	0.9	13.1	0.9	24.7	0.5
B1.2	5–10	Ah2	6.4	0	23.0	23.4	98.4	0.0	0.8	6.8	8.9	1.0	14.0	1.0	25.4	0.6
B1.3	10–15	ABh	6.3	0	20.3	20.6	98.5	0.0	0.6	5.3	8.7	1.2	15.3	1.0	24.5	0.6
B1.4	15–20	Bh	6.4	0	16.9	17.2	98.4	0.0	0.5	4.3	8.5	1.4	17.9	1.2	26.8	0.7
B1.5	20–25	B1	6.4	0	15.2	15.5	98.3	0.0	0.4	3.4	8.3	1.2	15.3	1.2	26.3	0.6
B1.6	25–40	B2	6.3	0	11.8	12.0	98.2	0.0	0.3	2.3	7.8	1.3	13.8	1.4	29.9	0.5
B2.1	0–5	Ah1	5.7	0	23.5	23.8	98.7	0.0	0.9	8.3	9.2	1.6	17.6	1.3	20.2	0.9
B2.2	5–10	Ah2	5.7	0	18.4	18.6	98.8	0.0	0.8	7.3	9.3	1.6	20.8	1.5	25.1	0.8
B2.3	10–15	ABh	5.8	0	18.8	19.1	98.9	0.0	0.7	6.1	9.2	1.7	21.5	1.5	26.0	0.8
B2.4	15–20	Bh1	5.8	0	16.9	17.3	97.6	0.0	0.5	5.1	9.4	1.7	22.4	1.5	25.3	0.9
B2.5	20–25	Bh2	5.9	0	14.6	14.7	98.9	0.0	0.4	4.1	9.5	1.6	20.9	1.6	30.1	0.7
B2.6	25–40	BC	6.5	0	12.8	13.1	98.0	0.0	0.3	2.7	9.0	0.9	15.5	1.0	22.1	0.7
B3.1	0–5	Ah1	5.0	0	13.5	14.5	93.0	0.0	1.1	9.4	8.8	2.0	21.4	1.7	17.4	1.2
B3.2	5–10	Ah2	5.3	0	11.3	12.0	94.4	0.0	0.6	5.3	8.9	2.0	20.8	1.8	25.6	0.8
B3.3	10–15	ABh	5.1	0	12.3	12.9	95.3	0.0	0.5	5.1	9.4	1.9	21.1	1.8	26.3	0.8
B3.4	15–20	Bh	5.2	0	13.4	14.4	93.2	0.0	0.5	4.5	9.4	1.9	26.7	1.6	27.5	1.0
B3.5	20–25	B1	5.3	0	12.5	12.9	97.0	0.0	0.4	3.8	8.8	1.6	17.9	1.6	26.6	0.7
B3.6	25–30	B2	5.2	0	12.1	12.5	96.8	0.0	0.4	3.4	9.0	1.3	14.2	1.5	26.7	0.5
B3.7	30–37	BC	6.4	0	12.0	12.3	97.7	0.0	0.3	2.4	8.6	0.9	12.1	1.2	25.4	0.5

Genetic horizons; characterised according to FAO (2006).

Ca_{Exch}, Al_{Exch}: exchangeable Ca and Al.

CEC_{sum}: cation exchange capacity calculated as the sum of exchangeable cations, not including H⁺.

TON, SOC and C:N ratio: total nitrogen, soil organic carbon and the ratio of the two

Fe_o, Al_o: oxalate-extractable Fe and Al.

Fe_d, Al_d: dithionite-extractable Fe and Al.

(Fig. 4). CEC_{SUM} was also higher at the CaCO₃-bearing (16.6 ± 1.9 cmol_c kg⁻¹) than at the CaCO₃-free site (4.3 ± 0.6 cmol_c kg⁻¹). This difference reflected the higher Ca_{Exch} content (Suppl. Fig. 2) at the CaCO₃-bearing site (16.1 ± 2.1 cmol_c kg⁻¹) relative to the CaCO₃-free site (3.2 ± 0.8 cmol_c kg⁻¹), as Ca was the predominant exchangeable cation at both sites. The Ca saturation of the exchange complex was high at both sites, but was greatest and had a smaller range at the CaCO₃-bearing site (93–99%) than at the CaCO₃-free site (48–93%). This difference was reflected in corresponding increases in Al saturation, as exchangeable Al (Al_{Exch}) was consistently detected at the CaCO₃-free site only.

Extraction efficiency of Ca increased in the order of H₂O < KCl ≈ Cohex < EDTA < CuCl₂. 2 M KCl extracted similar amounts of Ca as 0.0166 M Cohex at both sites, indicating that these two extracts effectively targeted the classical, exchangeable pool. The EDTA and CuCl₂ also extracted the exchangeable Ca pool at the CaCO₃-free site (Fig. 4), but extracted more Ca at the CaCO₃-bearing site, particularly in the samples with higher CaCO₃ contents.

3.3. Multivariate exploration of texture and mineralogy

Correlation analysis (Fig. 5) showed that there was a strong positive correlation between CaCO₃ and total Ca. There was also a strong positive correlation between CEC_{SUM} and Ca_{Exch}. On the other hand, there was a strong anti-correlation between Ca_{Exch}/Ca saturation and Al_{Exch}/Al saturation. Strong anti-correlations were also detected between fine silt and fine sand/clay contents, reflecting the fact that soil texture was dominated by silt populations, which exerted a ‘dilution’ effect (Bern, 2009) on other size classes (simplex behaviour). Total Mg and total Ca were also significantly anti-correlated with changes in total Si, which dominated major element composition, highlighting another ‘dilution’ effect.

A PCA (Suppl. Fig. 3A) followed by a factor analysis (Suppl. Fig. 3B) demonstrated that sites were clearly split along multivariate factor 1 (Suppl. Fig. 3C). This factor represented the abundance of Ca (as shown by the correlation with total Ca, CaCO₃ and Ca_{Sat}) and the anti-correlation between total Ca / Mg and total Si / quartz. The second factor

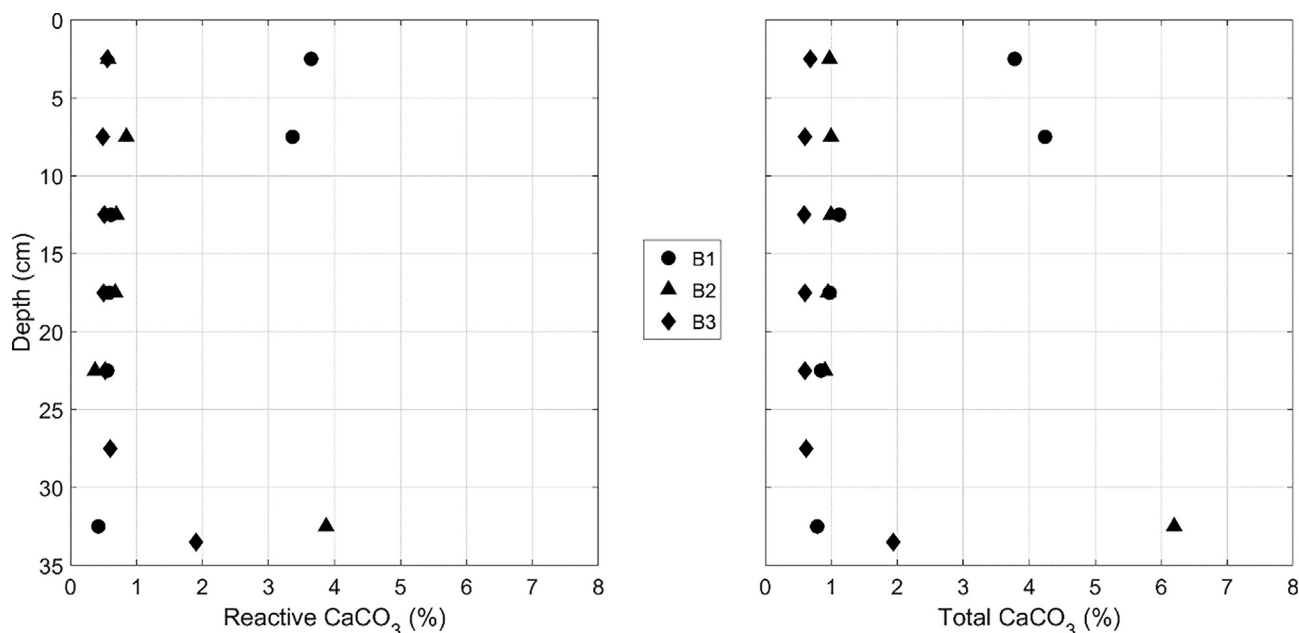


Fig. 3. Reactive and total contents of calcium carbonate equivalent for CaCO₃-bearing profiles (B1, B2, B3). Calcium carbonate equivalent contents were below the limits of detection at the CaCO₃-free site.

was a proxy for texture. There was no difference between sites along this factor, except for the fact that observations from the CaCO₃-free site showed a higher dispersion (had both lower and higher scores than observations from the CaCO₃-bearing site). Thus, overall differences in texture and silicate mineralogy were relatively small, but there were clear differences related to the presence or absence of CaCO₃, which differentiated the sites (Suppl. Fig. 3C).

3.4. Organic matter and free Al and Fe

Al_o was lower at the CaCO₃-bearing site (1.5 ± 0.2 g kg⁻¹) than at the CaCO₃-free (2.8 ± 0.2 g kg⁻¹), and did not vary with depth. Al_o displayed a strong negative correlation with pH (Fig. 6; R² = 0.88). Al_d was generally equal to Al_o at the CaCO₃-bearing site, suggesting that dithionite and oxalate quantitatively extracted the same Al pool. Al_d was however higher than Al_o at the CaCO₃-free site, suggesting that some Al substitution (Al incorporation into the crystalline lattice of Fe oxides dissolved by the dithionite treatment) had taken place.

Extractable Fe was an order of magnitude higher than extractable Al at both sites. There was an effect of depth on the amount of Fe_o, which became larger mid-profile (15–20 cm). There was also a significant influence of depth on the proportion of oxalate-to-dithionite extractable Fe, which typically decreased with depth, except for samples at

15–20 cm (Fig. 7). Both dithionite and oxalate extractable Fe were higher at the CaCO₃-bearing site (Fe_d = 25.3 ± 0.3 g kg⁻¹; Fe_o = 18.2 ± 1.6 g kg⁻¹) than at the CaCO₃-free (Fe_d = 22.7 ± 0.4 g kg⁻¹; Fe_o = 10.9 ± 0.5 g kg⁻¹). The proportion of oxalate-to-dithionite extractable Fe was also higher at the CaCO₃-bearing site (0.73 ± 0.06) than the CaCO₃-free (0.48 ± 0.01). Thus, extractable Fe was more abundant and predominantly found in poorly crystalline or monomeric forms at the CaCO₃-bearing site.

Organic carbon contents of AGB were similar between the sites (Suppl. Fig. 4). AGB estimates, reported in Blattner, were 281 g m⁻² at the CaCO₃-bearing sites and 350 g m⁻² at the CaCO₃-free site. We thus calculated that above-ground C amounted to 110 g C m⁻² at the CaCO₃-bearing site and 140 g C m⁻² at the CaCO₃-free site.

In contrast, SOC was approximately twice as high at the CaCO₃-bearing site (5.2 ± 0.2%) compared to the CaCO₃-free soils (2.5 ± 0.1%), decreasing systematically with depth at both sites (Fig. 8). SOC decreased with depth more linearly at the CaCO₃-bearing site (RMSE of linear relationship = 3.36) than at the CaCO₃-free (RMSE = 6.76; Suppl. Fig. 5A:C). The distribution of residuals from the linear relationship between SOC and depth at the CaCO₃-bearing site were normally distributed (p = 0.69), while the residuals at the CaCO₃-free site were not (p = 0.02). Total nitrogen followed an almost identical pattern and was thus higher at the CaCO₃-bearing site

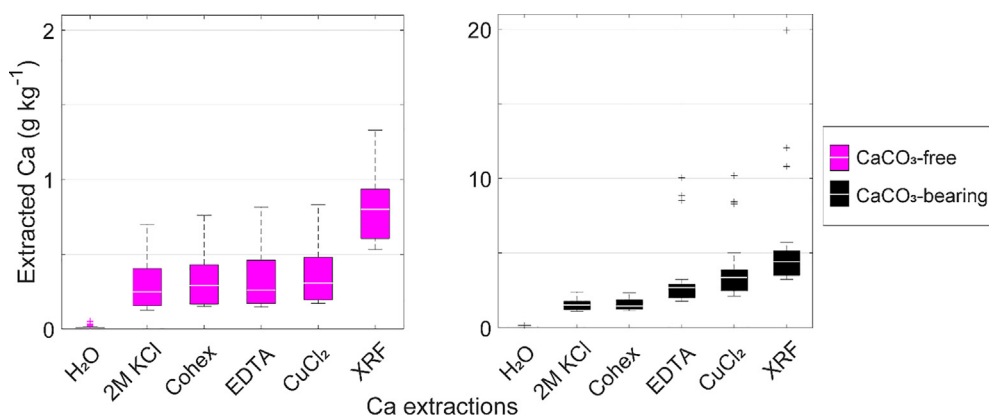


Fig. 4. Calcium content of CaCO₃-free and CaCO₃-bearing profiles. From left to right are deionised water, 2 M potassium chloride, 0.0166 M cobalt hexamine (Cohex), 0.05 M disodium EDTA and 0.5 M copper chloride extracts measured on an inductively coupled plasma optical emission spectrometer and total contents measured with X-ray fluorescence (XRF). Y scales differ by an order of magnitude. Bottom and top edges of the boxes in the box plot represent the 25th and 75th percentiles, the middle bars represent the median. Whiskers represent the range of most extreme data points not considered as outliers, while '+' represent outliers defined as values outside of the ± 2.7 standard deviation range.

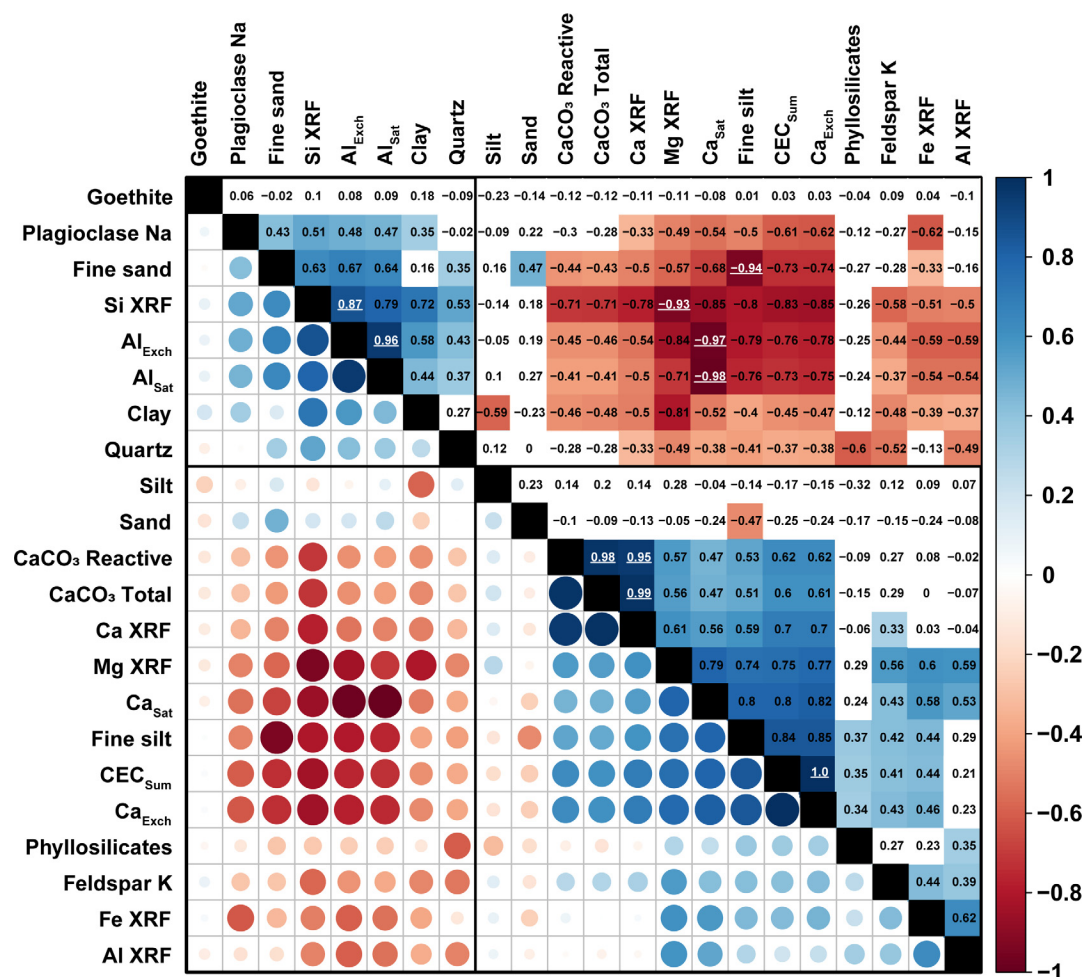


Fig. 5. Pearson's correlation coefficient matrix divided into two parts. The lower-left part represents the value of positive (blue) and negative (red) correlation coefficients as variations in circle size. The upper-right part displays the actual Pearson's correlation coefficients. Boxes in the upper-right part are only coloured in if the relationship is significant ($\alpha = 0.05$). Strong correlation coefficients are highlighted in white and underlined ($r \geq 0.85$). The different variables are hierarchically clustered using the complete-linkage method into two separate groups, highlighted with black rectangles in bold. (For interpretation of the references to colour in this figure legend, the reader is referred to the web version of this article.)

($0.6 \pm 0.0\%$) than at the CaCO_3 -free ($0.3 \pm 0.0\%$). Total N also decreased systematically with depth. The C:N ratio was low at both sites (Suppl. Fig. 6). It was slightly higher at the CaCO_3 -bearing site (8.9 ± 0.3) than at the CaCO_3 -free site (7.2 ± 0.3), but the differences were very small.

4. Discussion

In this study, we aimed to determine the influence of small amounts of CaCO_3 on pedogenesis and biogeochemistry. We used a naturally occurring gradient in CaCO_3 content affecting otherwise highly similar

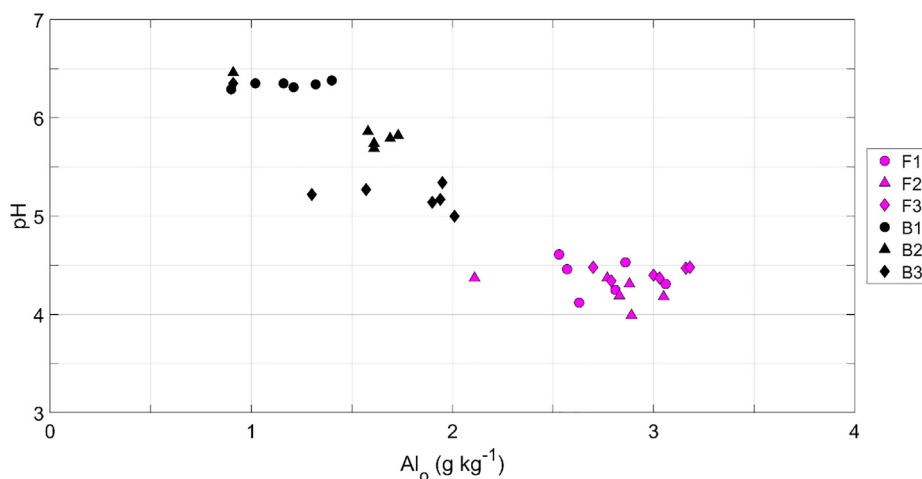


Fig. 6. Negative relationship between soil pH and oxalate extractable aluminium (Al_o) for CaCO_3 -free (F1, F2, F3) and CaCO_3 -bearing profiles (B1, B2, B3).

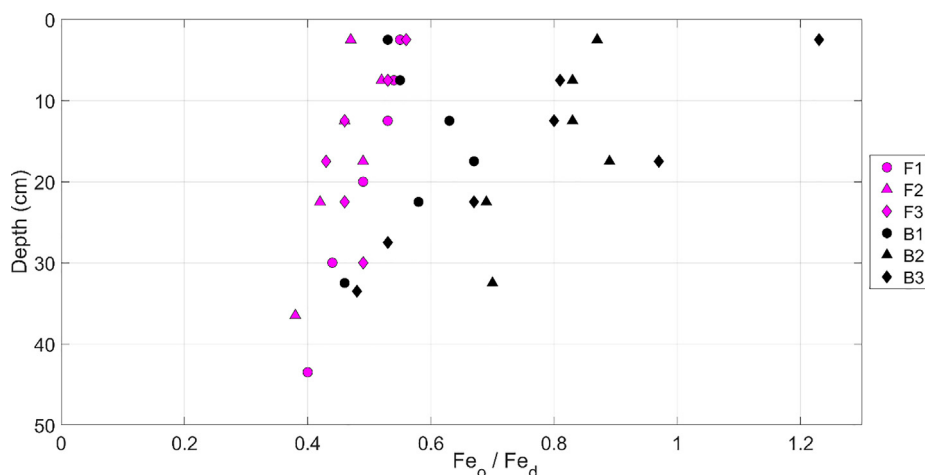


Fig. 7. Ratio between oxalate (Fe_o) and dithionite (Fe_d) extractable Fe contents for CaCO₃-free (F1, F2, F3) and CaCO₃-bearing (B1, B2, B3) profiles.

soils. With the constraints of finding near-identical soil forming conditions, we retained only 6 profiles, which were all located in close proximity (< 500 m). With such a low sample size, two things must be kept in mind:

- (1) The generalisation of findings to other soils is not supported by this experimental layout (but remains possible if a detailed mechanistic understanding is attained).
- (2) Only large effects could be statistically detected.

It was of prime importance that the soils be similar except for the presence/absence of CaCO₃, in order to isolate the role of CaCO₃ from other pedogenic variables. Homogeneity of parent material was of particular importance and is discussed further below.

4.1. Parent material

Textural analysis confirmed field observations that the parent material was homogeneous, with all samples plotting within the silt loam class. Both sites had 6 predominant textural populations, the modes of which are commonly encountered in previously glaciated landscapes (Boulton, 1978). The total composition of major elements were also similar between the sites. There was however a clear increase in Ca at the CaCO₃-bearing sites due to the presence of CaCO₃. This increase in Ca also caused a proportional decrease in Si (silicates) due to a ‘dilution’ effect. The slightly higher Mg content at the CaCO₃-bearing site could

be due to partial substitution of Mg for Ca in calcite (0.3% in measured coarse fragments) or the presence of poorly crystalline dolomite and accessory ferromagnesian minerals. P was also slightly elevated at the CaCO₃-bearing site, which could be a reflection of its lower mobility in Ca-bearing geochemical environments (von Wandruszka, 2006). K was marginally higher at the CaCO₃-bearing site and Na was higher at the CaCO₃-free site, which corresponded to small differences in K-feldspar and Na-plagioclase abundances, respectively. Relatively immobile elements such as Ti and other transition / post-transition metals showed near-uniform distribution between samples from different profiles, collected at different depths, pointing to a common source for parent materials. Neoformation of pedogenic clay was incipient at both sites, with only small quantities of an illite-vermiculite mixed-layer mineral detected (Egli et al., 2003; Zollinger et al., 2013). Most of the phyllosilicates originated from the physical disintegration of shale components of the Morcles Nappe.

While the siliceous component of the parent material at the two sites was near-homogeneous, there was a natural variation in CaCO₃ present at the alpage. This was likely due to the variability in CaCO₃ content of surficial deposits issued from the Morcles Nappe. The Grand Muveran cliffs protruding on the southeast side of the study area contain calcareous material, while the slopes of La Chaux on the northwest side essentially consist of shales. Thus, during the partial alluvio-colluvial reworking of the moraine and slope deposits that occurred following deglaciation, some carbonates were added to the CaCO₃-bearing site while little to no carbonates were added to the CaCO₃-free site.

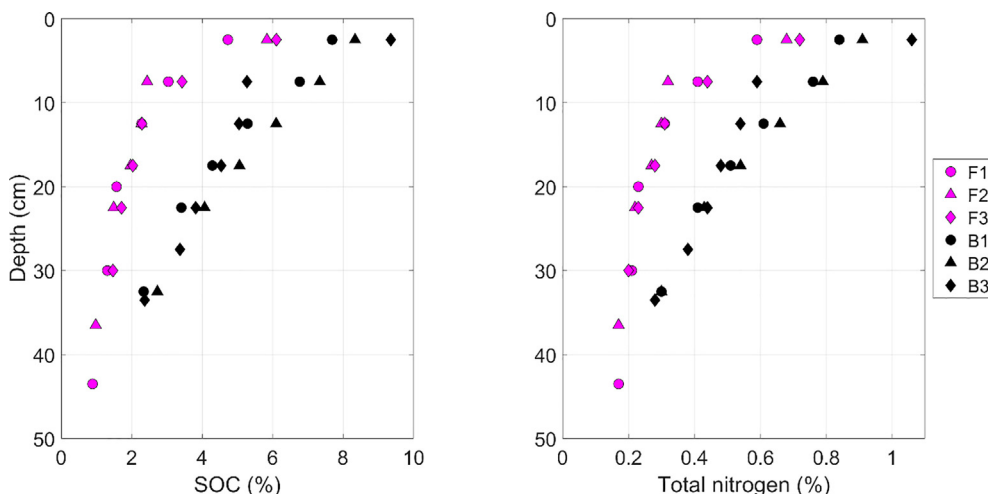


Fig. 8. Soil organic carbon (SOC) and total nitrogen contents for CaCO₃-free (F1, F2, F3) and CaCO₃-bearing (B1, B2, B3) profiles.

CaCO_3 was identified as being predominantly reactive at the Nant Valley (Fig. 3) by the adapted Loepfert et al. (1984) method. This method is not typically used for the measurement of reactive carbonates, but its results were in reasonable agreement with the EDTA extraction (Suppl. Fig. 7), which has been used previously for the estimation of reactive carbonates (Glover, 1961). Thus, CaCO_3 was most likely predominantly reactive at the CaCO_3 -bearing site, increasing the likelihood that it would play an active role in soil biogeochemistry.

Another difference between the sites was that free Fe forms were significantly less crystalline at the CaCO_3 -bearing profiles, relative to the CaCO_3 -free profiles. The sorption of organic colloids (Filimonova et al., 2016; Kleber and Jahn, 2007) and cations such as Ca_{Exch} (Thompson et al., 2011), which were more abundant at the CaCO_3 -bearing site, could have inhibited the formation of well-crystallised Fe forms. The increased pH at this site may have also indirectly influenced the crystallinity of Fe forms via its influence on their variable surface charge and their interaction with Ca_{Exch} (Schwertmann and Fechter, 1982), but this would still require further investigation. While the presence of CaCO_3 seemed to favour the prevalence of disordered Fe forms, the Fe_o/Fe_d ratio did not vary systematically with SOC, Ca_{Exch} or pH making it hazardous to attribute the differences in crystallinity to a single factor. It seems more likely that a mixture of indirect influences of CaCO_3 were involved in explaining the decreased crystallinity of Fe forms at the CaCO_3 -bearing site.

4.2. Accumulation of SOC

Soil organic carbon was approximately twice as high at the CaCO_3 -bearing site compared to the CaCO_3 -free site. A potential explanation for this accumulation could involve the higher primary productivity of grasses at the CaCO_3 -bearing site. Yet, AGB was slightly higher at the CaCO_3 -free site relative to the CaCO_3 -bearing site. Increased root turnover or exudation at the CaCO_3 -bearing site could explain part of the differences in SOC, but this effect should be relatively small due to the similarities between vegetation structure at the sites (Vittoz and Gmür, 2008). Instead, it was probably the difference in the efficiency of SOC stabilisation that drove the relative accumulation of SOC observed at the CaCO_3 -bearing site.

In a previous study, Grand et al. (2016) demonstrated that soil respiration was higher at the CaCO_3 -bearing site than the CaCO_3 -free site for 3 out of 4 of the measured months (July–Oct.); yet estimated heterotrophic respiration (Hanson et al., 2000) was actually lower throughout the entire measurement period, when expressed per unit SOC (Suppl. Table 3). This suggests that SOC at the CaCO_3 -bearing site has a certain biogeochemical stability, which may be contributing towards its accumulation (Whittinghill and Hobbie, 2012). Due to similarities between the sites, this stability cannot be explained by differences in texture or clay mineralogy. Potential geochemical controls that could influence the accumulation of SOC at the Nant Valley include the prevalence of reactive Ca and Fe forms, which are discussed further below.

4.2.1. Reactive Ca forms

We found a weak positive correlation between Ca_{Exch} and SOC at our sites (Suppl. Fig. 8C), which was particularly evident in the CaCO_3 -bearing profiles with higher pH and Ca_{Exch} . CEC_{sum} was also higher at the CaCO_3 -bearing sites (Suppl. Fig. 8D); this was partly attributable to the higher SOC content acting as loci for cation exchange, as clay mineralogy and texture were homogeneous at the sites. Thus, the commonly observed correlation between SOC and Ca_{Exch} could partially be explained by the increase in cation exchange sites provided by SOC (Briedis et al., 2012). However, there is evidence that Ca can also influence SOC dynamics (Groffman et al., 2006; Hobbie et al., 2002; Martí-Roura et al., 2019; Minick et al., 2017; Whittinghill and Hobbie, 2012) through several mechanisms (see Rowley et al., 2018 for more details). In our study, the two-fold increase in SOC at the CaCO_3 -

bearing site supports the hypothesis that reactive Ca is causally linked to the accumulation and stabilisation of SOC. Future investigation should focus on the mechanisms by which Ca influences SOC dynamics.

4.2.2. Analysing Ca forms

Exchangeable Ca may not be the only reactive Ca pool that influences SOC. It has been hypothesised that Ca could also stabilise SOC through inner sphere complexes (Rowley et al., 2018). This is supported by chemical modelling (Iskrenova-Tchoukova et al., 2010; Kalinichev and Kirkpatrick, 2007; Sutton et al., 2005), but as of yet, there is no direct evidence of this in soils. We attempted to extract this tightly bound, 'chelated Ca' pool using selective extractions, as has been done with the selective dissolution of free Fe and Al. Our more aggressive extracts, EDTA and CuCl_2 , yielded the same quantity of Ca as the exchangeable cations extracts (KCl/Cohex) at the CaCO_3 -free site, but more Ca than the exchangeable cations extracts at the CaCO_3 -bearing site. This was particularly apparent in samples with higher amounts of CaCO_3 and it thus seems as though both EDTA and CuCl_2 were aggressive towards reactive CaCO_3 , but failed to target Ca pools other than the exchangeable pool at CaCO_3 -free sites. Thus, the existence in soils of a tightly-bound Ca pool which is distinct from reactive CaCO_3 , and its selective extraction, remains an open question.

4.2.3. Fe forms

It is widely established that poorly crystalline Fe forms can stabilise SOC (Kögel-Knabner et al., 2008; von Lützow et al., 2006). In our study, SOC displayed a weak positive correlation with Fe_o , which was particularly evident in the profiles with the highest amounts of extractable Fe (Suppl. Fig. 8B). The same trend was observed for the degree of crystallinity of Fe oxides (Fe_o/Fe_d ; Suppl. Fig. 8A), as the amount of crystalline oxides was comparatively similar between profiles and it was mainly the amount of Fe_o that changed. The CaCO_3 -bearing profiles displayed an increase in Fe_o/Fe_d ratio mid-profile (15–20 cm; Fig. 7), potentially due to the mobility of poorly crystalline Fe species during brief suboxic events linked to snowmelt. It is possible that this pattern had some influence over the more linear SOC decline with depth at these sites (Suppl. Fig. 5A:C). Overall, our results support a positive relation between SOC accumulation and the amount of poorly crystalline Fe.

4.2.4. Ca and Fe interactions

It is interesting to note that our data hint at some kind of interaction or competition between Ca and Fe forms (Suppl. Fig. 8A:D). Profiles B1 and B2 showed no association between SOC and Fe_o , but were instead characterised by a strong correlation between SOC and Ca_{Exch} . On the contrary, in profile B3, where pH and CaCO_3 were slightly lower than in the other CaCO_3 -bearing profiles, SOC was significantly related to Fe_o and much less so to Ca_{Exch} . Speculatively, we propose that some organic functional groups may interact either with exchangeable cations or with reactive oxides depending on the prevailing biogeochemical conditions (pH and the prevalence of free elements), which may lead to a change in the relative importance of SOC stabilisation mechanisms (Rasmussen et al., 2018; Rowley et al., 2018).

Furthermore, a synergistic stabilisation of dissolved organic C by poorly crystalline Fe and Ca_{Exch} involving the formation of Fe-Ca-organic C ternary complexes, has recently been described (Sowers et al., 2018a,b). Hypothetically, this could also have exerted a positive feedback on the stabilisation of SOC at the CaCO_3 -bearing sites (Fig. 9), as disordered Fe forms that are favoured by the higher SOC, Ca_{Exch} and pH would in turn further contribute to an accumulation of SOC, rendered particularly effective by the presence of significant amounts of extractable Ca. This potential relationship between Ca and Fe and its impacts on SOC stabilisation and accumulation should now be investigated further in Ca-rich soils.

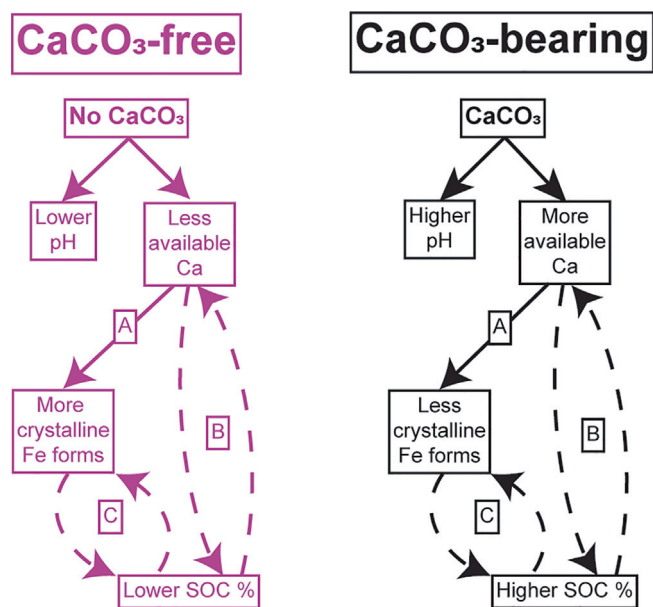


Fig. 9. A conceptual diagram of differences in biogeochemistry at the CaCO₃-free and CaCO₃-bearing sites, attributable to the cascading influence of CaCO₃. Direct interactions between geochemical variables are signified by straight arrows, while potential positive/negative feedback systems are signified by curved dashed arrows. The lettered interactions refer to: A) Ca-Fe interactions, where sorption of Ca by Fe oxides can prevent their further crystallisation (Thompson et al., 2011); B) Soil organic carbon (SOC)-Ca feedback loop, where SOC can be directly stabilised by Ca (Rowley et al., 2018), while SOC also provides exchange sites for the continued retention of available Ca forms; C) Fe-SOC feedback loop, where poorly crystalline Fe forms retain and stabilise SOC, while SOC can also inhibit the crystallisation of Fe forms (Kleber and Jahn, 2007).

4.3. Implications for modelling efforts

There is growing evidence that geochemical indicators are important parameters for modelling the persistence of SOC (Rasmussen et al., 2018; Vaughan et al., 2019). Indeed, models that infer SOC dynamics from clay content and climate would be unable to represent the difference in SOC content attributed here to the presence or absence of CaCO₃. Rasmussen et al. (2018) recently questioned the use of clay and climate as sole variables for modelling SOC and our results are in close agreement with their broader analysis of 5500 soil profiles. Models based on climate and clay content may be particularly inappropriate in situations where soil geochemistry is in disequilibrium with climate (occurrence of pedogenic inertia) and/or variations in types and crystallinity of Fe phases exist. Furthermore, modelling the depth distribution of SOC using an exponential decay function would have also misrepresented the different SOC-depth trends present at the sites, further underestimating SOC stocks at the CaCO₃-bearing site. These errors could however be reduced by accounting for differences in soil geochemistry and their subsequent effects on the accumulation of SOC and its depth distribution.

4.4. Synthesis – cascading biogeochemistry and the shift in geochemical controls on SOC stabilisation with pH

The divergence in biogeochemistry at the Nant Valley sites is caused by a state of pedogenic inertia, driven by the cascading influence of CaCO₃ dissolution (Fig. 9). The CaCO₃-bearing site exists in a state of disequilibrium with climate as the pedogenic threshold of CaCO₃ removal has not yet been breached. This threshold is unlikely to be breached in the near-future, due the presence of the adjacent calcareous cliffs and their alluvio-colluvial inputs, so that the site will likely

continue to retain its Mollic nature, high pH, and base saturation (Phaeozem).

Upon weathering, reactive CaCO₃ buffered pH levels (Likens et al., 1998), releasing Ca_{Exch} into the soil solution. This Ca_{Exch} can stabilise SOC (Oades, 1988; Rowley et al., 2018), which likely contributed to its accumulation in the CaCO₃-bearing profiles (x2). The presence of CaCO₃ also seemed to indirectly participate in the stabilisation of poorly crystalline Fe forms, which in turn, may have exerted a positive feedback on the retention of SOC, possibly involving ternary Fe-Ca-SOC complexes (Sowers et al., 2018a,b).

In contrast, the CaCO₃-free profiles had a lower pH. These acidic conditions in turn seemed to favour the prevalence of more crystalline Fe oxides such as goethite and higher amounts of reactive Al forms such as Al_{Exch} and Al_o (Adams et al., 2000). This confirms the long-held notion that decreasing soil pH identifies a shift along a weathering sequence from Ca-to-Al dominated biogeochemistry (Adams et al., 2000; Slessarev et al., 2016). In turn, this shift can be linked to different SOC stabilisation mechanisms (Rasmussen et al., 2018; Rowley et al., 2018), which could be used to help model the persistence of SOC. Thus, this study further supports the notion that soil pH could be used as an efficient and parsimonious variable for improving regional models of pedogenesis, biogeochemical functioning, and even SOC stabilisation (Clarholm and Skjellberg, 2013; Rowley et al., 2018). Future studies should investigate the potential of soil pH as a widely available indicator to account for the effects of geochemistry on SOC and improving the accuracy of regional SOC estimates.

Declaration of Competing Interest

The authors declare that they have no known competing financial interests or personal relationships that could have appeared to influence the work reported in this paper.

Acknowledgements

The authors would like to acknowledge Prof. Jasquelin Pena for the discussion that led to this paper. Thanks to Dr. Pascal Vittoz for many profitable discussions regarding the vegetation at the Nant Valley and *P. dactylifera*. Thanks to Dr. Magali Matteodo, Maité Buttet and Mélanie Delasoie for help with the sampling campaigns. Thanks to Dr. Jorge Spangenberg, Céline Blattner, Mélanie Delasoie and Franziska Fischer for help with measurements. Special thanks to the Canton de Vaud and IDYST for financially supporting this work and the “Conseil de Coordination Scientifique du Vallon de Nant, Université de Lausanne” for research permissions.

Appendix A. Supplementary data

Supplementary data to this article can be found online at <https://doi.org/10.1016/j.geoderma.2019.114065>.

References

- Adams, M.L., Hawke, D.J., Nilsson, N.H.S., Powell, K.J., 2000. The relationship between soil solution pH and Al³⁺ concentrations in a range of South Island (New Zealand) soils. *Soil Res.* 38 (1), 141–154.
- Adatte, T., Stinnesbeck, W., Keller, G., 1996. Lithostratigraphic and mineralogic correlations of near K/T boundary clastic sediments in northeastern Mexico: implications for origin and nature of deposition. *Geol. Soc. Am. Spec. Papers* 307.
- Aran, D., Maul, A., Masfaraud, J.-F., 2008. A spectrophotometric measurement of soil cation exchange capacity based on cobaltihexamine chloride absorbance. *C.R. Geosci.* 340 (12), 865–871.
- Arkley, R.J., 1963. Calculation of carbonate and water movement in soil from climatic data. *Soil Sci.* 96 (4), 239–248.
- Austin, N., Evans, B., Herwegh, M., Ebert, A., 2008. Strain localization in the Morcles nappe (Helvetic Alps, Switzerland). *Swiss J. Geosci.* 101 (2), 341–360.
- Bache, B.W., 1984. The role of calcium in buffering soils. *Plant, Cell Environ.* 7 (6), 391–395.
- Bahram, M., Hildebrand, F., Forslund, S.K., Anderson, J.L., Soudzilovskaia, N.A.,

- Bodegom, P.M., Bengtsson-Palme, J., Anslan, S., Coelho, L.P., Harend, H., Huerta-Cepas, J., Medema, M.H., Maltz, M.R., Mundra, S., Olsson, P.A., Pent, M., Pöhlme, S., Sunagawa, S., Ryberg, M., Tedersoo, L., Bork, P., 2018. Structure and function of the global topsoil microbiome. *Nature* 560 (7717), 233–237.
- Barra, C.M., Curtius, A.J., de Campos, R.C., Perez, D.V., 2001. Evaluation of four aluminum extraction methods using selected Brazilian soils. *Commun. Soil Sci. Plant Anal.* 32 (11–12), 1969–1980.
- Barta, G., Brádák, B., Novothny, Á., Markó, A., Szeberényi, J., Kiss, K., Kovács, J., 2018. The influence of paleogeomorphology on the stable isotope signals of paleosols. *Geoderma* 330, 221–231.
- Bartlett, R.J., James, B.R., 1993. Redox chemistry of soils. *Adv. Agron.* 50 (50), 151–208.
- Bern, C.R., 2009. Soil chemistry in lithologically diverse datasets: the quartz dilution effect. *Appl. Geochem.* 24 (8), 1429–1437.
- Bindschedler, S., Cailleau, G., Verrecchia, E., 2016. Role of fungi in the biomineralization of calcite. *Minerals* 6 (2), 41.
- Boulton, G.S., 1978. Boulder shapes and grain-size distributions of debris as indicators of transport paths through a glacier and till genesis. *Sedimentology* 25 (6), 773–799.
- Briedis, C., de Moraes Sá, J.C., Caires, E.F., de Fátima Navarro, J., Inagaki, T.M., Boer, A., de Oliveira Ferreira, A., Neto, C.Q., Canalli, L.B., Bürkner dos Santos, J., 2012. Changes in organic matter pools and increases in carbon sequestration in response to surface liming in an Oxisol under long-term no-till. *Soil Sci. Soc. Am. J.* 76 (1), 151–160.
- Bryan, W.H., Teakle, L.J.H., 1949. Pedogenic inertia: a concept in soil science. *Nature* 164, 969.
- Cailleau, G., Braissant, O., Dupraz, C., Aragno, M., Verrecchia, E.P., 2005. Biologically induced accumulations of CaCO₃ in orthox soils of Biga, Ivory Coast. *Catena* 59 (1), 1–17.
- Cerling, T.E., 1984. The stable isotopic composition of modern soil carbonate and its relationship to climate. *Earth Planet. Sci. Lett.* 71 (2), 229–240.
- Chadwick, O.A., Chorover, J., 2001. The chemistry of pedogenic thresholds. *Geoderma* 100 (3–4), 321–353.
- Clarholm, M., Skjellberg, U., 2013. Translocation of metals by trees and fungi regulates pH, soil organic matter turnover and nitrogen availability in acidic forest soils. *Soil Biol. Biochem.* 63, 142–153.
- Dahlgren, R.A., 1994. Quantification of allophane and imogolite. In: J.E. Amonette, Y.L. W. (Eds.), *Quantitative methods in soil mineralogy*. Soil Science Society of America, Madison, WI, pp. 430–451.
- Edwards, A.P., Bremner, J.M., 1967. Microaggregates in soil. *J. Soil Sci.* 18 (1), 64.
- Egü, M., Mirabella, A., Fitze, P., 2003. Formation rates of smectites derived from two Holocene chronosequences in the Swiss Alps. *Geoderma* 117 (1), 81–98.
- ESRI, 2019. World Imagery and national geographic base maps. ESRI, pp. World imagery “Sources: Esri, DigitalGlobe, GeoEye, i-cubed, USDA FSA, USGS, AEX, Getmapping, Aerogrid, IGN, IGP, swisstopo, and the GIS User Community” / National geographic “Sources: National Geographic, Esri, DeLorme, HERE, UNEP-WCMC, USGS, NASA, ESA, METI, NRCAN, GEBCO, NOAA, iPC”.
- FAO, 2006. Guidelines for soil description. FAO - Food and Agriculture Organization of the United Nations, Rome.
- Filimonova, S., Kauffhold, S., Wagner, F.E., Häusler, W., Kögel-Knabner, I., 2016. The role of allophane nano-structure and Fe oxide speciation for hosting soil organic matter in an allophanic Andosol. *Geochimica et Cosmochimica Acta* 180, 284–302.
- Galecki, A., Burzykowski, T., 2015. Linear mixed-effects models using R: A step-by-step approach. Springer New York, New York.
- Gao, Y., Tian, J., Pang, Y., Liu, J., 2017. Soil inorganic carbon sequestration following afforestation is probably induced by pedogenic carbonate formation in Northwest China. *Front. Plant Sci.* 8 (1282).
- Glover, E.D., 1961. Method of solution of calcareous materials using the complexing agent, EDTA. *J. Sedimentary Res.* 31 (4), 622–626.
- Grand, S., Rubin, A., Verrecchia, E.P., Vittoz, P., 2016. Variation in soil respiration across soil and vegetation types in an alpine valley. *PLoS ONE* 11 (9), e0163968.
- Grant, C.D., Dexter, A.R., Oades, J.M., 1992. Residual effects of additions of calcium compounds on soil structure and strength. *Soil Tillage Res.* 22 (3), 283–297.
- Groffman, P.M., Fisk, M.C., Driscoll, C.T., Likens, G.E., Fahey, T.J., Eagar, C., Pardo, L.H., 2006. Calcium additions and microbial nitrogen cycle processes in a Northern Hardwood Forest. *Ecosystems* 9 (8), 1289–1305.
- Hanson, P.J., Edwards, N.T., Garten, C.T., Andrews, J.A., 2000. Separating root and soil microbial contributions to soil respiration: A review of methods and observations. *Biogeochemistry* 48 (1), 115–146.
- Harris, D., Horwath, W.R., van Kessel, C., 2001. Acid fumigation of soils to remove carbonates prior to total organic carbon or carbon-13 isotopic analysis. *Soil Sci. Soc. Am. J.* 65 (6), 1853–1856.
- Hasinger, O., Spangenberg, J.E., Millière, L., Bindschedler, S., Cailleau, G., Verrecchia, E.P., 2015. Carbon dioxide in scree slope deposits: A pathway from atmosphere to pedogenic carbonate. *Geoderma* 247–248, 129–139.
- Hobbie, S.E., Miley, T.A., Weiss, M.S., 2002. Carbon and nitrogen cycling in soils from acidic and nonacidic tundra with different glacial histories in Northern Alaska. *Ecosystems* 5 (8), 0761–0774.
- Iskrenova-Tchoukova, E., Kalinichev, A.G., Kirkpatrick, R.J., 2010. Metal cation complexation with natural organic matter in aqueous solutions: molecular dynamics simulations and potentials of mean force. *Langmuir* 26 (20), 15909–15919.
- IUSS Working Group WRB, 2015. World reference base for soil resources 2014, update 2015. No 106. FAO, Rome.
- Jenny, H., 1941. Factors of soil formation: a system of quantitative pedology. McGraw-Hill, University of Michigan.
- Kalinichev, A.G., Kirkpatrick, R.J., 2007. Molecular dynamics simulation of cationic complexation with natural organic matter. *Eur. J. Soil Sci.* 58 (4), 909–917.
- Keeney, D.R., Nelson, D.W., 1982. Nitrogen in organic forms. In: A.L.e.a. Page (Ed.), *Methods of soil analysis*. American Society of Agronomy, Madison, WI.
- Kleber, M., Jahn, R., 2007. Andosols and soils with andic properties in the German soil taxonomy. *J. Plant Nutr. Soil Sci.* 170 (3), 317–328.
- Kögel-Knabner, I., Guggenberger, G., Kleber, M., Kandeler, E., Kalbitz, K., Scheu, S., Eusterhues, K., Leinweber, P., 2008. Organo-mineral associations in temperate soils: Integrating biology, mineralogy, and organic matter chemistry. *J. Plant Nutr. Soil Sci.-Zeitschrift Fur Pflanzenernahrung Und Bodenkunde* 171 (1), 61–82.
- Kowalska, J.B., Zaleski, T., Józefowska, A., Mazurek, R., 2019. Soil formation on calcium carbonate-rich parent material in the outer Carpathian Mountains – a case study. *Catena* 174, 436–451.
- Likens, G.E., Driscoll, C.T., Buso, D.C., Siccama, T.G., Johnson, C.E., Lovett, G.M., Fahey, T.J., Reiners, W.A., Ryan, D.F., Martin, C.W., Bailey, S.W., 1998. The biogeochemistry of calcium at Hubbard Brook. *Biogeochemistry* 41 (2), 89–173.
- Lo, I.M.C., Yang, X.Y., 1999. EDTA extraction of heavy metals from different soil fractions and synthetic soils. *Water Air Soil Pollut.* 109 (1), 219–236.
- Loeppert, R.H., Hallmark, C.T., Koshy, M.M., 1984. Routine procedure for rapid determination of soil carbonates. *Soil Sci. Soc. Am. J.* 48 (5), 1030–1033.
- Loeppert, R.H., Suarez, D.L., 1996. Carbonate and gypsum. In: D.L. Sparks, A.L. Page, P.A. Helmke, R.H. Loeppert (Eds.), *Methods of soil analysis part 3—chemical methods*. SSSA Book Series. Soil Science Society of America, American Society of Agronomy, Madison, WI.
- Marti-Roura, M., Hagedorn, F., Rovira, P., Romanyà, J., 2019. Effect of land use and carbonates on organic matter stabilization and microbial communities in Mediterranean soils. *Geoderma* 351, 103–115.
- McKeague, J.A., Day, D.H., 1966. Dithionite- and oxalate-extractable Fe and Al as aids in differentiating various classes of soils. *Can. J. Soil Sci.* 46 (1), 13.
- Mehra, O.P., Jackson, M.L., 1958. Iron oxide removal from soils and clays by a dithionite-citrate system buffered with sodium bicarbonate. *Clays Clay Miner.* 7 (1), 317–327.
- Minick, K.J., Fisk, M.C., Groffman, P.M., 2017. Soil Ca alters processes contributing to C and N retention in the Oa/A horizon of a northern hardwood forest. *Biogeochemistry* 1–15.
- Muhs, D.R., 1984. Intrinsic thresholds in soil systems. *Phys. Geogr.* 5 (2), 99–110.
- Munee, M., Oades, J.M., 1989. The role of Ca-organic interactions in soil aggregate stability. 3. Mechanisms and models. *Aust. J. Soil Res.* 27 (2), 411–423.
- Neuhaas, J.O., Wrigley, C., 1954. The quartimax rotation. *Br. J. Statistical Psychol.* 7 (2), 81–91.
- Oades, J.M., 1988. The retention of organic matter in soils. *Biogeochemistry* 5 (1), 35–70.
- Pansu, M., Gautheryou, J., 2006. *Handbook of Soil Analysis: Mineralogical, Organic and Inorganic Methods*. Springer, Berlin; New York.
- Perret, A., Martin, S., 2014. Carte Géomorphologique Du Vallon De Nant & Étude De La Marge Proglaciaire Du Glacier Des Martinets. *Bulletin Annuel De La Murithienne* 132, 69–82.
- R, 2019. R: A language and environment for statistical computing. In: R.C. Team (Ed.). R Foundation for Statistical Computing, Vienna, Austria.
- Ramnarine, R., Voroney, R.P., Wagner-Riddle, C., Dunfield, K.E., 2011. Carbonate removal by acid fumigation for measuring the $\delta^{13}C$ of soil organic carbon. *Can. J. Soil Sci.* 91 (2), 247–250.
- Rasmussen, C., Heckman, K., Wieder, W.R., Keiluweit, M., Lawrence, C.R., Berhe, A.A., Blankinship, J.C., Crow, S.E., Druhan, J.L., Hicks Pries, C.E., Marin-Spiotta, E., Plante, A.F., Schädler, C., Schimel, J.P., Sierra, C.A., Thompson, A., Wagai, R., 2018. Beyond clay: towards an improved set of variables for predicting soil organic matter content. *Biogeochemistry* 137 (3), 297–306.
- Rennett, T., 2019. Wet-chemical extractions to characterise pedogenic Al and Fe species – a critical review. *Soil Res.* 57 (1), 1–16.
- Rousk, J., Baath, E., Brookes, P.C., Lauber, C.L., Lozupone, C., Caporaso, J.G., Knight, R., Fierer, N., 2010. Soil bacterial and fungal communities across a pH gradient in an arable soil. *Int. Soc. Microbiol. Ecol. J.* 4 (10), 1340–1351.
- Rowley, M.C., Grand, S., Verrecchia, É.P., 2018. Calcium-mediated stabilisation of soil organic carbon. *Biogeochemistry* 137 (1), 27–49.
- Sanderman, J., 2012. Can management induced changes in the carbonate system drive soil carbon sequestration? A review with particular focus on Australia. *Agric. Ecosyst. Environ.* 155, 70–77.
- Satterthwaite, F.E., 1946. An approximate distribution of estimates of variance components. *Biometrics Bull.* 2 (6), 110–114.
- Schwertmann, U., Fechter, H., 1982. The point of zero charge of natural and synthetic ferrihydrites and its relation to adsorbed silicate. *Clay Miner.* 17 (4), 471–476.
- Seguinot, J., Juvet, G., Huss, M., Funk, M., Ivy-Ochs, S., Preusser, F., 2018. Modelling last glacial cycle ice dynamics in the Alps. *Cryosphere Discuss.* 2018, 1–30.
- Skjemstad, J., Fitzpatrick, R., Zarcinas, B., Thompson, C., 1992. Genesis of podzols on coastal dunes in southern Queensland. II. Geochemistry and forms of elements as deduced from various soil extraction procedures. *J. Soil Res.* 30 (5), 615–644.
- Slessarev, E.W., Lin, Y., Bingham, N.L., Johnson, J.E., Dai, Y., Schimel, J.P., Chadwick, O.A., 2016. Water balance creates a threshold in soil pH at the global scale. *Nature* 540 (7634), 567–569.
- Sørensen, T.J., 1948. A method of establishing groups of equal amplitude in plant sociology based on similarity of species content and its application to analyses of the vegetation on Danish commons. I kommission hos E. Munksgaard, København.
- Sowers, T., Adhikari, D., Wang, J., Yang, Y., Sparks, D.L., 2018a. Spatial associations and chemical composition of organic carbon sequestered in Fe, Ca, and organic carbon ternary systems. *Environ. Sci. Technol.*
- Sowers, T.D., Stuckey, J.W., Sparks, D.L., 2018b. The synergistic effect of calcium on organic carbon sequestration to ferrihydrite. *Geochem. Trans.* 19, 4.
- Sposito, G., 2016. *The Chemistry of Soils*. 3rd ed. Oxford University Press, Oxford.
- Sutton, R., Sposito, G., Diallo, M.S., Schulten, H.-R., 2005. Molecular simulation of a model of dissolved organic matter. *Environ. Toxicol. Chem.* 24 (8), 1902–1911.
- Thompson, A., Rancourt, D.G., Chadwick, O.A., Chorover, J., 2011. Iron solid-phase

- differentiation along a redox gradient in basaltic soils. *Geochim. Cosmochim. Acta* 75 (1), 119–133.
- Tirmizi, S.A., Wattoo, F.H., Wattoo, M.H.S., Khokhar, N.M., Iqbal, J., 2006. Analytical investigation of soil inorganic elements in cotton cultivated areas of Vehari - Pakistan. *J. Chem. Soc. Pak.* 27 (6), 606–610.
- van Reeuwijk, L.P., 2002. Procedures for soil analysis. 6th ed. FOA - Food and Agriculture Organization of United Nations: International Soil Reference and information Center (ISRIC), Wageningen, The Netherlands.
- Vaughan, E., Matos, M., Ríos, S., Santiago, C., Marín-Spiotta, E., 2019. Clay and climate are poor predictors of regional-scale soil carbon storage in the US Caribbean. *Geoderma* 354, 113841.
- Vittoz, P., Gmür, P., 2008. Introduction aux Journées de la biodiversité dans le Vallon de Nant. In: A.-C.P. Clot, D. Cherix, F. Dessimox, J.-L. Gattolliat, P. Gmür, P. Vittoz, M. Vust (Eds.), Biodiversité du Vallon de Nant Premières Journées de la biodiversité en Suisse romande (5 et 6 juillet, 2008) Mémoire Vol 23. Société vaudoise des Sciences naturelles, Vaud, Switzerland.
- von Lützw, M., Kögel-Knabner, I., Ekschmitt, K., Matzner, E., Guggenberger, G., Marschner, B., Flessa, H., 2006. Stabilization of organic matter in temperate soils: mechanisms and their relevance under different soil conditions - a review. *Eur. J. Soil Sci.* 57 (4), 426–445.
- von Wandruszka, R., 2006. Phosphorus retention in calcareous soils and the effect of organic matter on its mobility. *Geochem. Trans.* 7 (1), 6.
- Webster, R., 2007. Analysis of variance, inference, multiple comparisons and sampling effects in soil research. *Eur. J. Soil Sci.* 58 (1), 74–82.
- Wei, T., Simko, V., 2017. R package “corrplot”: Visualization of a Correlation Matrix.
- Whittinghill, K.A., Hobbie, S.E., 2012. Effects of pH and calcium on soil organic matter dynamics in Alaskan tundra. *Biogeochemistry* 111 (1–3), 569–581.
- Zamanian, K., Pustovoytov, K., Kuzyakov, Y., 2016. Pedogenic carbonates: forms and formation processes. *Earth Sci. Rev.* 157, 1–17.
- Zollinger, B., Alewell, C., Kneisel, C., Meusbürger, K., Gaertner, H., Brandova, D., Ivy-Ochs, S., Schmidt, M.W.I., Egli, M., 2013. Effect of permafrost on the formation of soil organic carbon pools and their physical-chemical properties in the Eastern Swiss Alps. *Catena* 110, 70–85.